Journal of Materials Chemistry A

COMMUNICATION

Check for updates

Cite this: J. Mater. Chem. A, 2018, 6, 23263

Received 25th August 2018
Accepted 17th October 2018

DOI: 10.1039/c8ta08259f

rsc.li/materials-a

Synthesis of mesoporous Fe_3Si aerogel as a photothermal material for highly efficient and stable corrosive-water evaporation†

Fengyu Zhang,[a] Yaguang Li,*[a] Xianhua Bai,[a] Shufang Wang,[a] Baolai Liang,[a] Guangsheng Fu[a] and Zhong-Shuai Wu*[b]

Synthesis of photothermal materials with high efficiency and anti-corrosion stability is key for photothermal corrosive-water evaporation, but remains a great challenge. Herein, for the first time, we developed mesoporous Fe_3Si aerogel as a new photothermal material for remarkably efficient and stable corrosive-water evaporation. The as-prepared Fe_3Si aerogel presented narrow mesopores with a size of 2–3 nm that could greatly reduce the thermal conductivity to 0.04 W m^{-1} K^{-1}, which is the lowest reported value so far, and depressed the latent heat of water evaporation. The obtained Fe_3Si aerogel supported on melamine foam demonstrated outstanding seawater evaporation rate of 2.08 kg m^{-2} h^{-1} and high solar-thermal utilization efficiency of 91.8% under one solar level irradiation, exceeding those of most of the photothermal materials. Notably, owing to the strong corrosion resistance, the support-free hydrophobic Fe_3Si aerogel displayed utrastable solar-thermal water evaporation performance, with more than 1 kg m^{-2} h^{-1} of water evaporation and outstanding cycling stability in two highly corrosive solutions, namely, 0.5 M H_2SO_4 and 1 M NaOH. Therefore, we believe that the Fe_3Si aerogels have great potential for wide industrial applications such as seawater desalination, salt production, brine management and water purification.

Introduction

Fresh water is one of nature's most important gifts to mankind and is essential for our survival.[1] However, the current drinking water is being overly contaminated, resulting in the serious shortage of fresh water.[2] Corrosive water (*e.g.*, seawater) is a nearly unlimited source for fresh water production.[3] Converting solar energy to heat by photothermal materials for water evaporation has been gradually recognized as a green and promising way for seawater desalination and other corrosive-water evaporation.[4,5] In this regard, one great challenging issue is to simultaneously improve the water evaporation efficiency and stability of photothermal materials.[6,7] Thus far, more studies have focused on increasing sunlight absorption with black photothermal materials, such as metallic nanoparticles and carbon based materials, to convert more heat for promoting water evaporation efficiency.[8–12] However, most reported photothermal materials have generally presented high thermal conductivity.[13,14] In such cases, sunlight-converted heat energy was partly lost to the air, by thermal conduction of the photothermal materials instead of being used for water evaporation.[15,16] It is known that appropriately tuning the porous structure can decrease the thermal conductivity of photothermal materials.[16] However, the size of pores reported for photothermal materials are at micrometer level, which could reduce the thermal conductivity to only 10 W m^{-1} K^{-1}.[13,14,17–19] Apart from the requirement of improved water evaporation efficiency, photothermal materials should possess excellent anti-corrosion properties towards corrosive solutions, such as acids and bases, to extend their applications in different media.[20–24] Nevertheless, rational design and fabrication of such a stable photothermal material with wide wavelength range for light absorption and extremely low thermal conduction remains elusive.

In this study, we report a novel, inexpensive photothermal material, Fe_3Si aerogel, with properties such as narrow mesopores of 2–3 nm size, full absorption of sunlight, and outstanding anti-corrosion resistance, as a new photothermal material for highly efficient and stable water evaporation from various types of corrosive solutions. Importantly, the mesoporous structure of the Fe_3Si aerogel could greatly reduce the thermal conductivity to 0.04 W m^{-1} K^{-1}, which is the lowest value reported for photothermal materials, and even well comparable to thermally insulating foams.[25,26] As a result, our

[a]Hebei Key Lab of Optic-electronic Information and Materials, The College of Physics Science and Technology, Hebei University, Baoding, 071002, China. E-mail: yaguang_1987@126.com

[b]Dalian National Laboratory for Clean Energy, Dalian Institute of Chemical Physics, Chinese Academy of Sciences, 457 Zhongshan Road, Dalian 116023, China. E-mail: wuzs@dicp.ac.cn

† Electronic supplementary information (ESI) available. See DOI: 10.1039/c8ta08259f

Fe_3Si aerogels exhibited excellent thermal storage capacity. Additionally, the Fe_3Si aerogel supported on melamine foam showed outstanding seawater evaporation rate of 2.08 kg m^{-2} h^{-1} and superior solar-thermal efficiency of 91.8% under one solar irradiation, exceeding the traditional theoretical limit of photo-thermal water evaporation.[16] Remarkably, Fe_3Si aerogel was stable not only in seawater but also in highly corrosive systems (*e.g.*, H_2SO_4, NaOH) for efficient photothermal water evaporation due to its excellent corrosion resistance.

Experimental section

Chemicals

Fe_3Si particles and melamine foam were purchased from CHINO new material ltd. and Zhengzhou SHIKE Co., Ltd. respectively. Ethylsilicate (TEOS), polyethylene glycol (PEG 2000), *n*-heptane, ammonia, glucose and NaCl were purchased from Kermel. All chemicals, including hydrochloric acid (YaoHua chemical industry), alcohol (FengChuan chemical industry), iron nitrate (Fuchen chemical industry), and trimethylchlorosilane (Macklin), were used without further treatment.

Synthesis of Fe_3Si aerogel

First, 10 mL TEOS was mixed with 40 mL alcohol. Subsequently 0.33 mL concentrated hydrochloric acid and 0.7 mL deionized water were added to the above mixed solution. After stirring, the obtained solution was transferred to a heated plate and stirred for 4 h at 85 °C and then, 10 g PEG 2000 and 3 g ferric nitrate were added; after dissolving them, 5 mL ammonium hydroxide was rapidly added into the solution. Then, the resulting sample was aged for 3 days at 65 °C, and directly annealed at 500 °C for 6 h in air. Then, the obtained Fe-doped SiO_2 aerogel was grinded to powder and annealed in H_2 atmosphere with 100 sccm at 400 °C for 3 h. Finally, Fe_3Si aerogels were obtained. For comparison, we also synthesized pure SiO_2 aerogel, using the same procedure but without adding Fe precursor.

Seawater evaporation

Simulated seawater comprising pure water with 3.5 wt% NaCl was used in this experiment. The glass Petri dish with diameter of 42 mm and depth of 11 mm was placed on the electronic balance as seawater container. Then, 11 mL seawater was added to this Petri dish. Melamine foam of 40 mm diameter and 9 mm thickness was chosen as the support for Fe_3Si aerogels (50 mg),[27] which were coated on the top surface of melamine foam, about 2 mm higher than the surface of seawater. Then, the Petri dish was illuminated by a simulated solar light source (xenon lamp, Perfectlight Co., Ltd, Fig. S1†) with 1.0 kW m^{-2} power (power at center of water surface). The water evaporation mass was recorded by an electronic balance with precision of 0.01 g.

Hydrophobic modification of Fe_3Si aerogel

Self-floatable hydrophobic Fe_3Si aerogel was prepared for highly corrosive-water evaporation. In this case, Fe_3Si aerogel was treated with trimethylchlorosilane *n*-heptane solution for 72 hours, and the samples were dried at 200 °C in the air for 12 hours.

Corrosive water evaporation

The concentration of sulfuric acid and sodium hydroxide solutions were 0.5 and 1 M (mol L^{-1}), respectively. The glass (for H_2SO_4) and plastic (for NaOH) beakers of 40 mm diameter were placed on the electronic balance. Then, 50 mL of each corrosive solution was added into the corresponding beaker. Then, 50 mg hydrophobic Fe_3Si aerogel, free of melamine foam support, was added into each beaker and illuminated by simulated solar light source (xenon lamp) with 1.16 kW m^{-2} light intensity (center water surface power). The water evaporation data was recorded by the measurement from electronic balance. After five test cycles, the evaporated water mass was added in beakers again before the next five test cycles.

Characterizations

The as-prepared samples were studied by powder X-ray diffraction (XRD), which was performed on a Bede D1 system operated at 20 kV and 30 mA with Cu Kα radiation ($\lambda = 1.5406$ Å). Transmission electron microscopy (TEM, JEOL F200) was used to identify the morphology and crystallinity of the nanostructures, energy-dispersive X-ray spectroscopy (EDS) mapping was also performed. Scanning electron microscopy (SEM) images were obtained with the FEI Nova NanoSEM450 (Czech Republic, European Union). The Brunauer–Emmett–Teller (BET) surface area and pore size were measured by a Micromeritics Tristar 3030 system. Ultraviolet-visible-near infrared absorption spectrum was recorded on Hitachi Limited U4100 (Japan). Contact angle measurements were recorded to test the hydrophobic property using Data Physics OCA 15EC (Germany). Infrared (IR) images were obtained using a Fluke Ti300 infrared camera (America). The emissivity of Fe_3Si aerogel and bulk Fe_3Si was tested as follows. First, we placed the samples in dark environment and tested the temperature with a thermocouple. Then, we used the IR camera to test the temperature of materials. Next, we changed the emissivity of the IR camera to make the IR temperature equal to the temperature showed by thermocouple. The emissivity was corrected as 0.88 and 0.92 for Fe_3Si aerogel and bulk Fe_3Si, respectively.

Thermal conductivity calculations

Thermal conductivity (κ) was calculated based on $\kappa = D \times C_p \times d$,[28] where the thermal diffusivity D was measured using the laser flash technique in a Linseis LFA1000 system, the specific heat capacity C_p was measured using a Netzsch DSC200F3 differential scanning calorimeter, and the bulk density d was determined by measuring the dimensions and mass of the samples and then reconfirmed by the Archimedes method. We pressed 0.27 g pure bulk Fe_3Si particles and 0.03 g Fe_3Si aerogel to obtain standard disks at 12 MPa for 3 min. The calculated intensities of disk made by pure Fe_3Si particles and Fe_3Si aerogel were 4213 and 577 kg m^{-3}, respectively.

Results and discussion

Fig. 1a shows the synthesis scheme of Fe_3Si aerogel. First, the Fe-doped SiO_2 aerogel with high Fe dopant concentration (Fe/Si ratio = 1/6) was synthesized through a sol–gel process. XRD pattern revealed that the sample was in amorphous silica phase[29] (Fig. 1b) and SEM image showed porous particle morphology (Fig. 1c and d). The BET surface area of Fe-doped SiO_2 aerogel was 550 $m^2 g^{-1}$ and the average mesoporous size was 8.8 nm (Fig. S2a, b†). The Fe 2p XPS spectrum of Fe-doped SiO_2 aerogel showed two characteristic peaks of Fe $2p_{3/2}$ at 710.8 eV and Fe $2p_{1/2}$ at 725 eV, suggesting Fe(III) doping into SiO_2 aerogel (Fig. S2d†). Following this, black colored Fe_3Si aerogel was successfully prepared by annealing Fe-doped SiO_2 aerogel in hydrogen gas at 400 °C for 3 h. Fig. 1e shows the XRD pattern of the Fe_3Si aerogel. There are three sharp peaks at 45°, 65° and 82°, corresponding to the (110), (200) and (211) lattice planes of Fe_3Si (JCPDS 35-0519). A wide amorphous peak appearing at 23° verified the presence of amorphous SiO_2. Furthermore, the crystalline Fe_3Si phase well-wrapped by amorphous SiO_2 was revealed by the high resolution TEM image (Fig. S3a†). Additionally, SEM images of Fe_3Si aerogel exhibited a disordered and unsystematic particle morphology (Fig. 1f). A mesoporous structure could be clearly observed in high-magnification SEM image (Fig. 1g), similar to the morphology of pure SiO_2 aerogel (Fig. S3b†).

Nitrogen adsorption and desorption isotherms of Fe_3Si aerogel revealed a high BET surface area of 498 $m^2 g^{-1}$ (Fig. 2a), and narrow mesoporous size distribution of 2–3 nm (Fig. 2b),[30] caused by the volume expansion during the alloying process of Fe and Si. The temperature-dependent total thermal conductivity (k) for Fe_3Si aerogel is shown in Fig. 2c. The k value of bulk Fe_3Si with macropores was 15 W $m^{-1} K^{-1}$ (50–400 °C temperature range, Fig. S4†). Notably, the k value of Fe_3Si aerogel over the entire temperature range (50–400 °C) was about

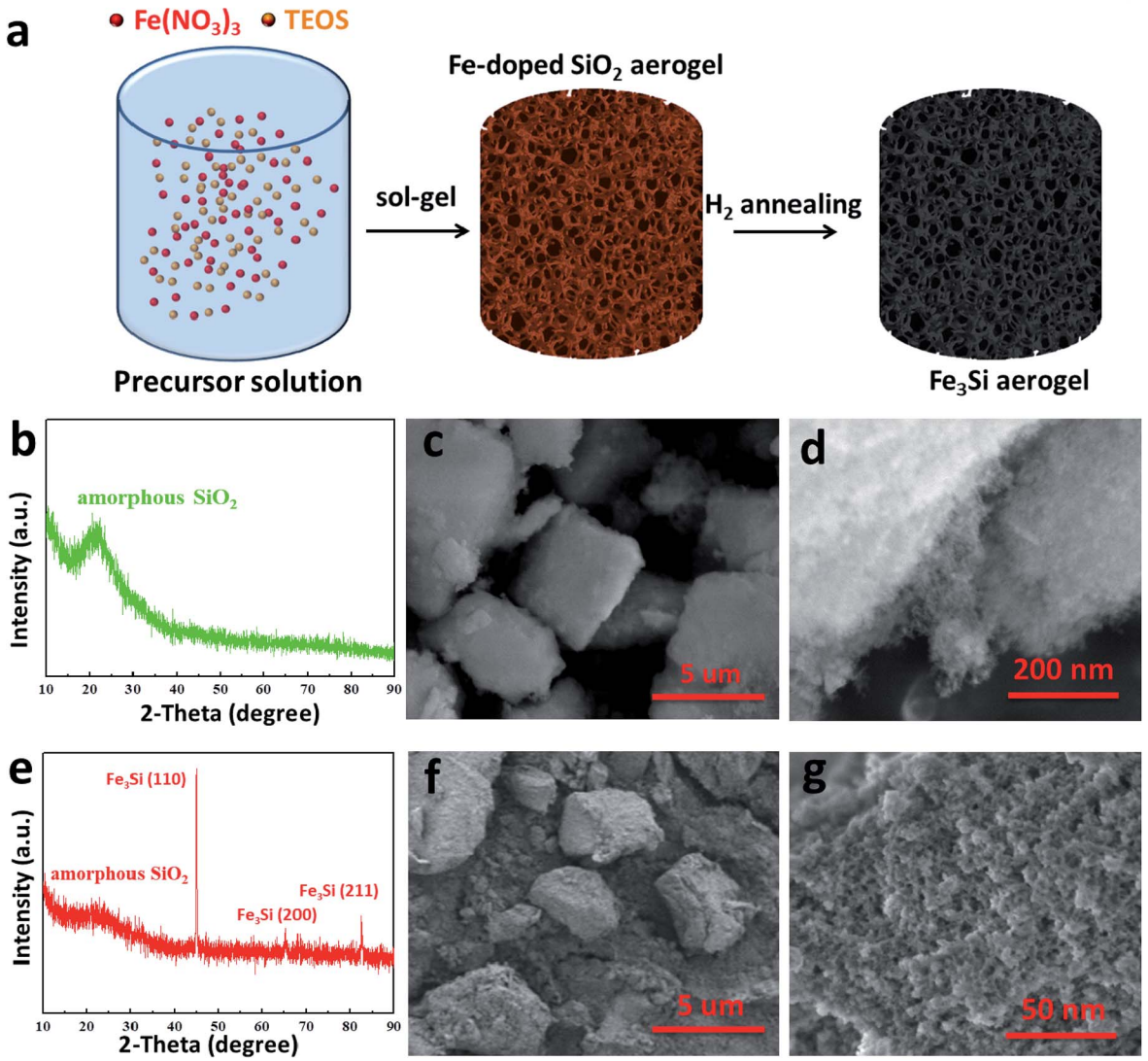

Fig. 1 (a) Schematic of the synthesis process for Fe_3Si aerogel. (b) XRD pattern, (c) SEM image, and (d) high-magnification SEM image of Fe-doped SiO_2 aerogel. (e) XRD pattern, (f) SEM image, and (g) high-magnification SEM image of as-fabricated Fe_3Si aerogel.

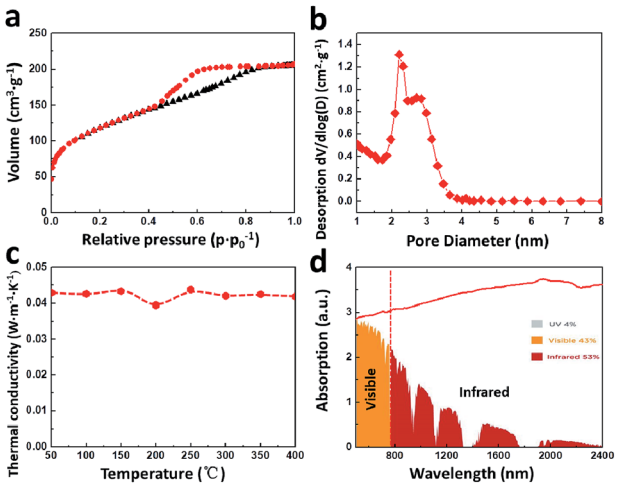

Fig. 2 (a) Nitrogen adsorption and desorption isotherms, (b) pore size distribution, (c) temperature-dependent total thermal conductivity and (d) ultraviolet-visible-near infrared absorption spectrum of mesoporous Fe_3Si aerogel.

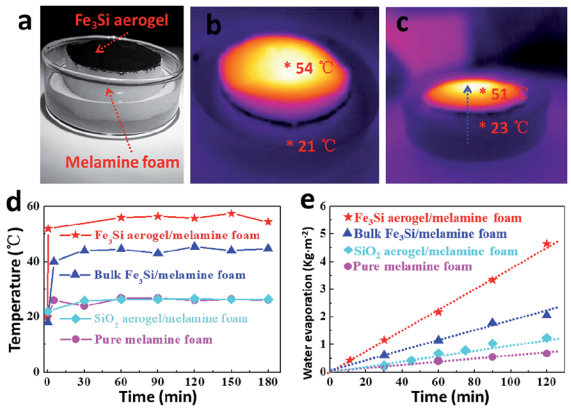

Fig. 3 (a) Photograph of Fe_3Si aerogel supported on melamine foam in solar-vapor desalination unit. (b, c) The corresponding top-view and side viewed infrared (IR) images (obtained by IR camera) in solar-vapor desalination unit after 5 minutes of 1.0 kW m^{-2} sunlight illumination. (d) The temperature evolution and (e) seawater evaporation performance of Fe_3Si aerogel, bulk Fe_3Si and pure SiO_2 aerogel supported on melamine foam under 1.0 kW m^{-2} solar illumination, in comparison with melamine foam only.

0.04 W m^{-1} K^{-1}, which was two orders of magnitudes lower than that of bulk Fe_3Si and very close to that of thermal insulators, *e.g.*, polystyrene foam (0.041 W m^{-1} K^{-1}).[31–34] This result confirmed that the narrow mesopores could significantly reduce the thermal conductivity of materials. It should be emphasized that as a black material, mesoporous Fe_3Si aerogel showed a full absorption of light from 500 nm to 2400 nm wavelength (Fig. 2d), displaying full sunlight absorption capacity. With the irradiation of 1.0 kW m^{-2} standard sunlight (one solar intensity), the temperature of pure Fe_3Si aerogel could be as high as 102 °C (Fig. S5†). To the best of our knowledge, Fe_3Si aerogel showed the highest surface temperature under one solar irradiation, demonstrating almost full conversion of light into heat energy.

To conduct photothermal seawater evaporation, we first coated mesoporous Fe_3Si aerogel on the top surface of the melamine foam (Fe_3Si aerogel/melamine foam, Fig. 3a). It should be noted that the top surface of the melamine foam was higher than the air-seawater interface to maintain the floatability of the Fe_3Si aerogel. A simulated sunlight source with 1.0 kW m^{-2} energy intensity was used to illuminate the Fe_3Si aerogel/melamine foam immersed in seawater. The top-view infrared (IR) picture showed the temperature of only 21 °C for seawater under sunlight irradiation, and of 54 °C for mesoporous Fe_3Si aerogel layer on melamine foam (Fig. 3b). Furthermore, the side-viewed IR picture exhibited a drastic temperature change from 51 °C for the Fe_3Si aerogel layer to 23 °C for the melamine foam (Fig. 3c). This suggested that the light converted to heat energy was mainly localized in the Fe_3Si aerogel layer. For comparison, we also synthesized and coated bulk Fe_3Si on melamine foam (bulk Fe_3Si/melamine foam, Fig. S6†). It was disclosed that with the increase in irradiation time, the surface temperature was stable at 52 °C for mesoporous Fe_3Si aerogel/melamine foam, which was much higher than that of bulk Fe_3Si/melamine foam (45 °C), SiO_2 aerogel/melamine foam (25 °C, Fig. S6e, f†) and individual melamine foam (25 °C) (Fig. 3d). As a result, the water evaporation rate of Fe_3Si aerogel/melamine foam was about 2.08 kg m^{-2} h^{-1} (Fig. 3e), which was 6.7 times higher than that of melamine foam (0.31 kg m^{-2} h^{-1}) and much higher than that of SiO_2 aerogel/melamine foam (0.53 kg m^{-2} h^{-1}) and most of the reported photothermal materials, *e.g.*, hollow carbon (1.45 kg m^{-2} h^{-1}),[35] graphene oxide/carbon nanotubes (1.25 kg m^{-2} h^{-1}),[36] graphene foam (1.4 kg m^{-2} h^{-1}),[37] Ti_2O_3 (1.32 kg m^{-2} h^{-1}),[38] and Mg reduced TiO_2 (0.8 kg m^{-2} h^{-1})[39] (Table S1†). It is worth noting that the seawater evaporation rate of hydrophobic Fe_3Si aerogel/melamine foam obtained even at a high interface temperature of 78 °C was only ~1.49 kg m^{-2} h^{-1} (Fig. S7†), which was about 71% of that of pristine Fe_3Si aerogel/melamine foam at the low temperature of 52 °C (2.08 kg m^{-2} h^{-1}, Fig. 3d, e). Notably, the water evaporation efficiency of Fe_3Si aerogel/melamine foam exceeded the traditional theoretical limit of photothermal water evaporation efficiency under one solar irradiation (≤1.5 kg m^{-2} h^{-1}).[7] This was mainly attributed to the reduction of the latent heat of water evaporation by confining the transport of small sized water clusters in the mesoporous channels.[40,41] To validate this, we tested the latent heat of seawater evaporation of mesoporous Fe_3Si aerogel/melamine foam, the obtained value was only 1520 kJ kg^{-1}, which was much lower than that obtained for bulk Fe_3Si/melamine foam (2215 kJ kg^{-1}) and for melamine foam (1909 kJ kg^{-1}) (Fig. S8†). Furthermore, the solar-thermal utilization efficiency of mesoporous Fe_3Si aerogel/melamine foam was as high as 91.8% (Fig. 3e), which was much higher than that of bulk Fe_3Si aerogel/melamine foam (70.7%), under same sunlight irradiation of 1.0 kW m^{-2} (Table S2†). Importantly, it was revealed that, under 1, 2 and 3 times of solar irradiation (1 to 3 kW m^{-2}), the seawater evaporation masses gradually

increased from 2.08 to 2.75 and 3.3 kg m^{-2} h^{-1} (Fig. S9†). These results demonstrated that the mesoporous Fe_3Si aerogel holds great potential for seawater evaporation.

Apart from seawater, the efficient evaporation of other corrosive liquids is also of wide significance in pure-water production, brine management, and pollutant treatment. Melamine foam is not stable in corrosive water; thus, it could not be used as a support for mesoporous Fe_3Si aerogel in H_2SO_4 and NaOH. Considering the fact that our mesoporous Fe_3Si aerogel presented high water-evaporation efficiency, strong acid/alkaline resistance, and anti-oxidation ability, we further examined the water evaporation performance of support-free, self-floatable hydrophobic mesoporous Fe_3Si aerogels in 0.5 M H_2SO_4 and 1 M NaOH. The monolith of pure Fe_3Si aerogel without hydrophobic treatment exhibited a low water contact angle of 33° (Fig. S10†). After hydrophobic modification, hydrophobic Fe_3Si aerogel demonstrated a high water contact angle of 110° (Fig. 4a) and in this case, all particles were readily floating on the surface of water (Fig. 4b). Fig. 4c and d exhibit the photograph and IR picture of hydrophobic Fe_3Si aerogel floating on the surface of H_2SO_4 solution under light irradiation (1.16 kW m^{-2} intensity). Notably, Fe_3Si aerogel presented excellent heat accumulation capacity, and a record air–water interface temperature of 84 °C, much higher than the maximum value reported (68 °C) in literature under similar sunlight irradiation.[7] In addition, the heat loss from thermal radiation for Fe_3Si aerogel was 0.44 kW m^{-2} in both 0.5 M H_2SO_4 and 1 M NaOH solutions (with surface temperature of 84 °C), which was significantly greater than that from the hydrophilic Fe_3Si aerogel/melamine foam in seawater (0.08 kW m^{-2}, 52 °C, see calculation details in ESI†).

After 3 hours of sunlight irradiation, the evaporated water amount in 0.5 M H_2SO_4 and 1 M NaOH reached 4.05 and 3.64 kg m^{-2}, respectively (Fig. 5a and b). To highlight the outstanding cycling stability, the first five cycles of photothermal water evaporation (each cycle conducted for 3 h) for hydrophobic Fe_3Si aerogels were conducted. The mass of water evaporation was verified to decrease from 4.05 to 3.57 kg m^{-2} in 0.5 M H_2SO_4 solution and from 3.64 to 3.08 kg m^{-2} in 1 M NaOH solution after the five cycles (Fig. 5c and d). Remarkably, with another 5 cycle-test, both solutions showed water evaporation performance similar to that of the first five cycles (Fig. S11†). This excellent cycling stability was attributed to the exceptional anti-corrosion properties of stable structure and high hydrophobic nature of the Fe_3Si aerogel (Fig. S12†). For comparison, we also tested the stability of porous carbon for corrosive water evaporation in H_2SO_4 and NaOH solutions (Fig. S13†). It was clearly seen that after 1 day, the porous carbon was completely deposited at the bottom of both H_2SO_4 and NaOH solutions, suggesting its inability for corrosive-water evaporation due to the poor anti-oxidation properties in alkaline and oxyacid solutions.[10,11,42] Hydrophobic Fe_3Si aerogel showed stable solar-thermal water evaporation efficiency of 1 kg m^{-2} h^{-1} in both highly corrosive systems, namely, 0.5 M H_2SO_4 and 1 M NaOH. This value is lower than that of Fe_3Si aerogel supported on melamine foam in seawater (2.08 kg m^{-2} h^{-1}). This low value of hydrophobic Fe_3Si aerogel is not only caused by the high interface temperature but also possibly by the increase in latent heat (2592–2697 kJ kg^{-1}) of corrosive-water evaporation, *e.g.*, H_2SO_4 solution (Fig. S14†), resulting from hydrophobic treatment and free support of Fe_3Si aerogel. These results demonstrated the wide industrial applicability of hydrophobic Fe_3Si aerogel in highly corrosive solutions. It is worth

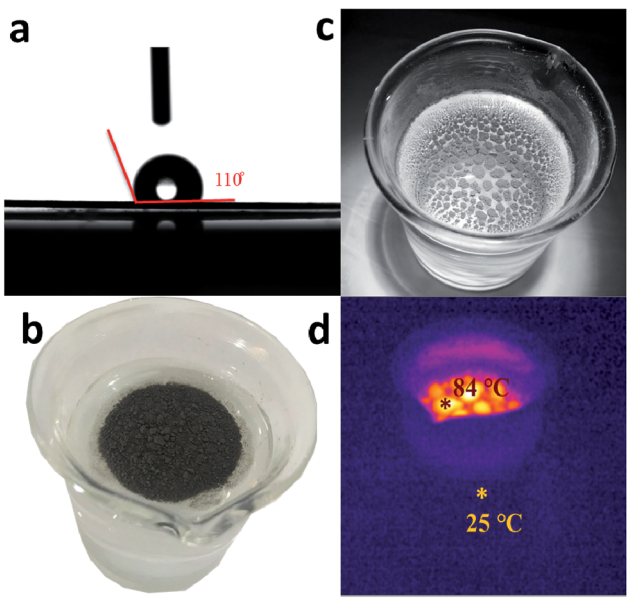

Fig. 4 The water contact angle of (a) hydrophobic Fe_3Si aerogel. A water droplet was loaded on the surface of a sample disc, which was prepared by pressing materials. (b) Photograph of the floating state of hydrophobic Fe_3Si aerogel. (c, d) Photograph and IR images of hydrophobic Fe_3Si aerogel floating on the surface of H_2SO_4 after 10 minutes of 1.16 kw m^{-2} sunlight illumination.

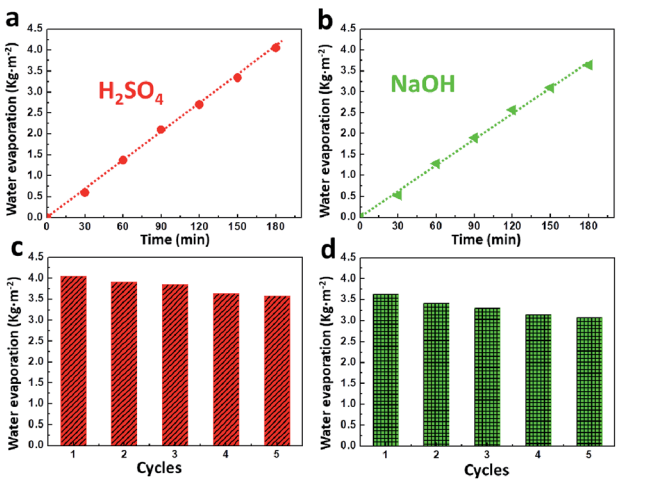

Fig. 5 (a, b) The water evaporation performances of hydrophobic Fe_3Si aerogel floated on (a) 0.5 M H_2SO_4 and (b) 1 M NaOH, under 1.16 kw m^{-2} solar illumination. (c, d) Cycling performances of hydrophobic Fe_3Si aerogel floated on (c) 0.5 M H_2SO_4 and (d) 1 M NaOH, under 1.16 kw m^{-2} solar illumination.

noting that this is the first demonstration of a photothermal material used for corrosive-water evaporation.

Conclusions

In summary, we synthesized an ultrastable and efficient photothermal material, *viz.*, mesoporous Fe_3Si aerogel, possessing outstanding anti-corrosion ability, full sunlight absorption (up to 2400 nm), low thermal conductivity (0.04 W m^{-1} K^{-1}) and the ability to reduce the latent heat of water evaporation. As a result, the as-synthesized Fe_3Si aerogel showed a record air–water interface temperature of 84 °C, exhibiting excellent thermal storage ability. Fe_3Si aerogel supported on melamine foam displayed unprecedented photothermal evaporation rate of 2.08 kg m^{-2} h^{-1} and solar-thermal utilization efficiency of 91.8% from seawater under 1.0 kW m^{-2} of sunlight irradiation. Importantly, our support-free hydrophobic Fe_3Si aerogels possessed superior corrosion resistance, outstanding water-evaporation efficiency (1 kg m^{-2} h^{-1}) and excellent cycling stability, and was the first demonstration of a photothermal material that could maintain stability in corrosive H_2SO_4 and NaOH solutions. Therefore, Fe_3Si aerogels have great potential for industrial applications in the direction of conversion of solar illumination into water evaporation in different complex environments.

Conflicts of interest

The authors declare no competing financial interest.

Acknowledgements

This study was supported by the Outstanding Youth Foundation of Hebei Province (Grant No. A2016201176), National Nature Science Foundation of China (Grant No. 51702078, 51572259, 51872283) and Outstanding Doctoral Cultivation Project of Hebei University (YB201502), National Key R&D Program of China (Grant 2016YFB0100100 and 2016YFA0200200), Recruitment Program of Global Expert (1000 Talent Plan), DICP (DICP ZZBS201708), DICP&QIBEBT (Grant DICP&QIBEBT UN201702), Dalian National Laboratory For Clean Energy (DNL), CAS.

References

1 D. Brogioli, R. Zhao and P. M. Biesheuvel, *Energy Environ. Sci.*, 2011, **4**, 772–777.
2 Z. Lianbin, T. Bo, W. Jinbo, L. Renyuan and W. Peng, *Adv. Mater.*, 2015, **27**, 4889–4894.
3 A. ElMekawy, H. M. Hegab and D. Pant, *Energy Environ. Sci.*, 2014, **7**, 3921–3933.
4 H. Rao, L. C. Schmidt, J. Bonin and M. Robert, *Nature*, 2017, **548**, 74–77.
5 M. Zhu, Y. Li, G. Chen, F. Jiang, Z. Yang, X. Luo, Y. Wang, S. D. Lacey, J. Dai, C. Wang, C. Jia, J. Wan, Y. Yao, A. Gong, B. Yang, Z. Yu, S. Das and L. Hu, *Adv. Mater.*, 2017, **29**, 1704107.
6 L. Zhang, B. Tang, J. Wu, R. Li and P. Wang, *Adv. Mater.*, 2015, **27**, 4889–4894.
7 Y. Zeng, J. Yao, B. A. Horri, K. Wang, Y. Wu, D. Li and H. Wang, *Energy Environ. Sci.*, 2011, **4**, 4074.
8 H. Ghasemi, G. Ni, A. M. Marconnet, J. Loomis, S. Yerci, N. Miljkovic and G. Chen, *Nat. Commun.*, 2014, **5**, 4449.
9 Y. Ito, Y. Tanabe, J. Han, T. Fujita, K. Tanigaki and M. Chen, *Adv. Mater.*, 2015, **27**, 4302–4307.
10 Y. Liu, J. Chen, D. Guo, M. Cao and L. Jiang, *ACS Appl. Mater. Interfaces*, 2015, **7**, 13645–13652.
11 A. S. U. Oara Neumann, J. Day, S. Lal, N. Peter and N. J. Halas, *ACS Nano*, 2013, **7**, 42–49.
12 K. Bae, G. Kang, S. K. Cho, W. Park, K. Kim and W. J. Padilla, *Nat. Commun.*, 2015, **6**, 10103.
13 I. Yoshikazu, T. Yoichi, H. Jiuhui, F. Takeshi, T. Katsumi and C. Mingwei, *Adv. Mater.*, 2015, **27**, 4302–4307.
14 X. Huang, K. Qian, J. Yang, J. Zhang, L. Li, C. Yu and D. Zhao, *Adv. Mater.*, 2012, **24**, 4419–4423.
15 G. Xue, K. Liu, Q. Chen, P. Yang, J. Li, T. Ding, J. Duan, B. Qi and J. Zhou, *ACS Appl. Mater. Interfaces*, 2017, **9**, 15052–15057.
16 T. Li, H. Liu, X. Zhao, G. Chen, J. Dai, G. Pastel, C. Jia, C. Chen, E. Hitz, D. Siddhartha and R. Yang, *Adv. Funct. Mater.*, 2018, **28**, 1707134.
17 X. Hu, W. Xu, L. Zhou, Y. Tan, Y. Wang, S. Zhu and J. Zhu, *Adv. Mater.*, 2017, **29**, 1604031.
18 J.-H. Lee, G. A. Galli and J. C. Grossman, *Nano Lett.*, 2008, **8**, 3750–3754.
19 Z. Yichi, D. Tristan, M. L. Snedaker, W. Heng, K. Stephan, C. S. Birkel, J. Xiulei, L. Deyu, S. G. Jeffrey and G. D. Stucky, *Adv. Mater.*, 2012, **24**, 5065–5070.
20 G. Xue, Y. Xu, T. Ding, J. Li, J. Yin, W. Fei, Y. Cao, J. Yu, L. Yuan, L. Gong, J. Chen, S. Deng, J. Zhou and W. Guo, *Nat. Nanotechnol.*, 2017, **12**, 317.
21 L. Shi, Y. Wang, L. Zhang and P. Wang, *J. Mater. Chem. A*, 2017, **5**, 16212–16219.
22 Ö. Kılıc and A. M. Kılıc, *Desalination*, 2005, **186**, 11–19.
23 K. Manzoor, S. J. Khan, Y. Jamal and M. A. Shahzad, *Chem. Eng. Res. Des.*, 2017, **118**, 226–237.
24 D. Xevgenos, K. Moustakas, D. Malamis and M. Loizidou, *Desalin. Water Treat.*, 2014, **57**, 2304–2314.
25 V. Vaou and D. Panias, *Miner. Eng.*, 2010, **23**, 1146–1151.
26 E. Placido, M. C. Arduini-Schuster and J. Kuhn, *Infrared Phys. Technol.*, 2005, **46**, 219–231.
27 L. Qinghua, L. Zhi, Y. Xiaoliang, H. Zheng-Hong, K. Feiyu and Y. Quan-Hong, *Adv. Mater.*, 2015, **27**, 4634–4639.
28 K. Ahn, M.-K. Han, J. He and J. Androulakis, *J. Am. Chem. Soc.*, 2010, **132**, 5227–5235.
29 W. Xu, T. Ollevier and F. Kleitz, *ACS Catal.*, 2018, **8**, 1932–1944.
30 V. O. Williams, N. C. Jeong, C. Prasittichai, O. K. Farha, M. J. Pellin and J. T. Hupp, *ACS Nano*, 2012, **6**, 6185–6196.
31 S. U. S. Choi, *ASME Fluids Eng.*, 1995, **231**, 99–105.
32 J. Kuhn, *Int. J. Heat Mass Transfer*, 1992, **35**, 1795–1801.
33 J. H. Blackwell, *J. Appl. Phys.*, 1954, **25**, 137–144.
34 A. M. Papadopaulos, *ScienceDirect*, 2005, **37**, 77–86.

35 J. Zhou, Z. Sun, M. Chen, J. Wang, W. Qiao, D. Long and L. Ling, *Adv. Funct. Mater.*, 2016, **26**, 5368–5375.
36 Y. Li, T. Gao, Z. Yang, C. Chen, W. Luo, J. Song, E. Hitz, C. Jia, Y. Zhou, B. Liu, B. Yang and L. Hu, *Adv. Mater.*, 2017, **29**, 1700981.
37 H. Ren, M. Tang, B. Guan, K. Wang, J. Yang, F. Wang, M. Wang, J. Shan, Z. Chen, D. Wei, H. Peng and Z. Liu, *Adv. Mater.*, 2017, **26**, 1702590.
38 J. Wang, Y. Li, L. Deng, N. Wei, Y. Weng, S. Dong, D. Qi, J. Qiu, X. Chen and T. Wu, *Adv. Mater.*, 2017, **29**, 1603730.
39 M. Ye, J. Jia, Z. Wu, C. Qian, R. Chen, P. G. O'Brien, W. Sun, Y. Dong and G. A. Ozin, *Adv. Energy Mater.*, 2017, **7**, 01811.
40 X. Zhou, F. Zhao, Y. Guo, Y. Zhang and G. Yu, *Energy Environ. Sci.*, 2018, **11**, 1985–1992.
41 F. Zhao, J. Bae, X. Zhou, Y. Guo and G. Yu, *Adv. Mater.*, 2018, 1801796.
42 H. Sun, Z. Xu and C. Gao, *Adv. Mater.*, 2013, **25**, 2554–2560.